Topography Analysis and Homogeneity Quantification of Laser-Patterned Periodic Surface Structures

Marcos Soldera[*1], Charlotte Reichel[1], Florian Kuisat[1], Andrés Fabián Lasagni[1,2]

[1]Institut für Fertigungstechnik, Technische Universität Dresden, George-Bähr-Str. 3c, 01069 Dresden, Germany
[2]Fraunhofer-Institut für Werkstoff- und Strahltechnik IWS, Winterbergstr. 28, 01277 Dresden, Germany
[*]*Corresponding author's e-mail: marcos.soldera@tu-dresden.de*

Functionalization of surfaces by engraving micro or nano-textures using laser-based methods has become a broad field of research with potential for large-scale manufacturing. Particularly, Direct Laser Interference Patterning (DLIP) is a surface structuring method that allows the fabrication of periodic structures with resolutions down to the micro- or submicron scale with throughputs even over 1 m^2/min. However, the production of large areas with high texture quality and reproducibility is still challenging. One of the reasons for this, is the lack of an objective methodology to quantify the texture homogeneity so that different processing conditions can be compared to find the optimum laser process window. In this study, a statistical analysis based on the Gini coefficient is employed to quantitatively assess the homogeneity of DLIP-produced textures on three coating systems. The method allowed for an objective comparison of the impact of the process conditions on the different materials. For instance, it was observed that within the set of studied parameters the number of applied pulses has a higher impact on the texture homogeneity than the fluence per pulse and that the optimum number of pulses for the studied process lies between 10 and 20.
DOI: 10.2961/jlmn.2022.02.2002
Keywords: Direct Laser Interference Patterning, homogeneity assessment, hard coatings, surface structuring, Gini coefficient

1. Introduction

Functionalization of surfaces by engraving micro or nanotextures has become a broad field of research with potential for industrial deployment [1,2]. Particularly, laser-based methods offer a unique combination of flexibility, high resolution, high throughput, and environmental-friendly by-products [3,4]. Among these methods, Direct Laser Interference Patterning (DLIP) is able to fabricate periodic surface structures with resolutions down to the micro- or submicron scale with throughputs even over 1 m^2/min [5,6]. In DLIP two or more laser beams are overlapped onto the sample surface to produce an interference pattern with a periodic intensity distribution. If the local intensity is sufficiently high, the material can be ablated or melted at the maxima positions leaving a repetitive topography on the surface. The texture geometry can be controlled with high flexibility by adjusting the number of interfering beams, their polarization, and overlapping angles [7,8]. Additionally, the spatial period can be easily controlled by fine-tuning the overlapping angle between the beams or changing the working wavelength [9].

One of the current challenges for this technique is to ensure a sufficiently good texture homogeneity over large areas so that the produced functionality can be controlled on the entire workpiece. In this context, reliable methodologies for quantifying the homogeneity of periodic textures are required as a first step for designing process control schemes. Traditional surface roughness parameters like Root Mean Square (RMS) roughness or average height cannot be used unequivocally to characterize periodic topographies because those parameters cannot distinguish a deviation from the average value due to the induced periodic modulation or due to surface imperfections [10,11]. To circumvent the limitations of traditional roughness parameters to assess the homogeneity of periodic surfaces, several methods were developed for specific surface textures [12–22]. According to these reports, these approaches were able to provide a quantification of the texture homogeneity and allowed a comparison between textures with similar characteristics. However, they were either designed for particular texture geometries or they are not robust enough because user-defined parameters must be arbitrarily defined [11].

Recently, a statistical analysis based on the Gini coefficient was developed for periodic surfaces [11,23], whereby the homogeneity can be objectively assessed in terms of a set of attributes, such as the structure height. The Gini analysis has been extensively used to characterize the inequality of a society, typically in terms of income distribution of the population [24,25]. The output of this method is the Gini coefficient G, a figure of merit that oscillates between zero and one depending on the degree of inequality. For a perfect equal population $G = 0$, while for an absolute inequal distribution $G = 1$. When the method is applied to periodic topographies, the calculated homogeneity is inversely proportional to the Gini coefficient. Furthermore, the authors state this approach can be easily adapted to different texture geometries including 2D periodic structures. Although this method has the potential to become a robust tool for surface characterization, it has not been exploited

thoroughly. Thus, in this contribution DLIP-structured hard coatings with varying aspect ratios were analyzed with the Gini coefficient theory to establish a correlation between the DLIP-irradiation conditions and the resulting surface homogeneity.

2. Materials and methods

2.1 Samples preparation

Three coatings systems, namely CrN (chromium nitride), WC (tungsten carbide), and a-C:H (amorphous hydrogenated carbon), were studied in this work. The coatings were deposited on stainless steel plates using a combination of PVD (Physical Vapor Deposition), namely reactive magnetron sputtering, and PACVD (Plasma-Assisted Chemical Vapor Deposition) methods adding a thickness between 20 µm and 30 µm to the substrates. Details on the coatings deposition can be found elsewhere [26–28].

The samples were structured by two-beam DLIP employing a solid-state laser source (Edgewave PX2000) emitting radiation with a wavelength of 1064 nm, a pulse duration of 10 ps, and a repetition rate of 10 kHz. In the DLIP optical module, the primary beam is divided by a diffractive optical element (DOE) into two beams of comparable intensities. Then, the beams are parallelized by a prism and finally overlapped with a lens on the substrate, yielding line-like textures with a nominal spatial period of 5.8 µm for all samples. Different structure heights and texture uniformities were achieved depending on the used laser parameters, namely fluence per pulse and number of applied pulses. The diameter of the interference area was approximately 196 µm. The fluence threshold was calculated with the D^2 method applying one pulse per position, yielding 0.36 J/cm^2 (WC), 0.32 J/cm^2 (CrN) and 0.51 J/cm^2 (a-C:H). Further experimental details of the used DLIP system can be found in Ref. [26].

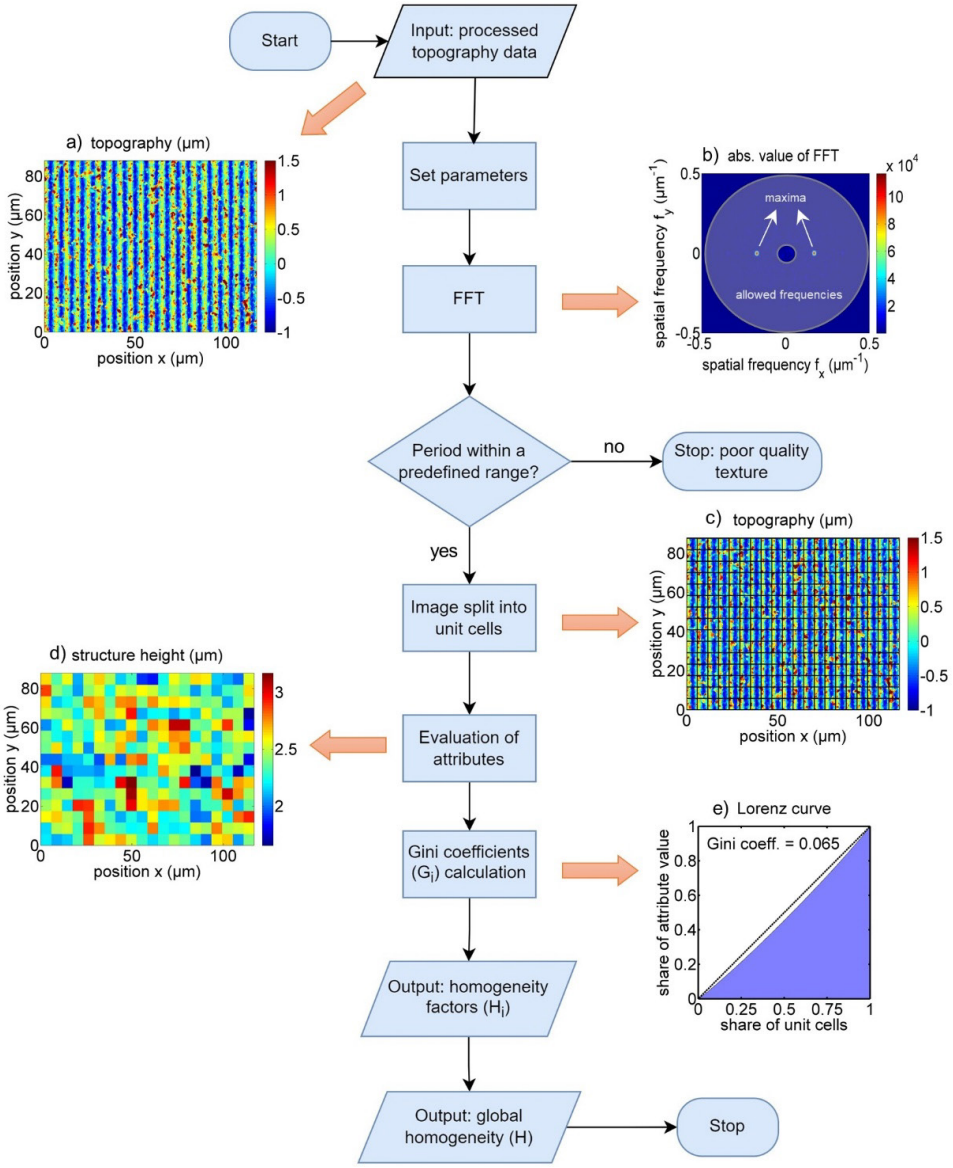

Fig. 1 Flowchart describing the algorithm used to implement the Gini analysis in MATLAB together with exemplary images (a-e) produced during the execution of the code.

2.2 Topography characterization

The topography of the laser-treated surfaces was measured by optical confocal microscopy (Sensofar S–Neox) equipped with a 150X objective providing a vertical and lateral resolution of 1 nm and 140 nm, respectively. The measured topographies were post-processed with SensoMAP Advanced Analysis Software (Sensofar) to level the surface by the least squares plane method, eliminate high-frequency noise (data outliers), and fill non-measured pixels, if any.

3. Results and discussion

3.1 Development of an algorithm for the Gini analysis

The Gini analysis and homogeneity quantification were implemented in MATLAB with a self-developed script following the flowchart in Fig. 1. The algorithm uses as input the post-processed topography data from the confocal microscope of each sample. As an example, Fig. 1a shows the topography of a WC coating treated with 10 pulses with a fluence of 0.87 J/cm^2 per pulse. After initializing the program, the fast-Fourier transform (FFT) algorithm is executed on the topography data Z(x,y). Next, the code searches for the maximum of the absolute value of the Fourier transform of the topography $\mathcal{F}$(Z(x,y)). If the maximum lies within a predefined range of allowed spatial frequencies, then the spatial period of the line-like texture can be extracted from the location of the maximum. In this study the maximum and minimum allowed spatial periods were 20 µm and 2 µm, corresponding to the spatial frequencies of 0.5 µm^{-1} and 0.05 µm^{-1}, respectively. This region of allowed spatial frequency is defined in Fig. 1b, between the concentric circles. If the maximum value of $\mathcal{F}$(Z(x,y)) is found outside the allowed spatial frequency range, then it is inferred that the texture is so inhomogeneous that there are no periodic structures but rather a random surface. In this case, the algorithm stops, concluding that the homogeneity is too low for quantification.

For good quality textures, the topography image is divided into square unit cells with an edge length equal to the spatial period (see Fig. 1c). This allows the evaluation of different topographical attributes of each unit cell according to the Gini analysis approach. In this work, three amplitude roughness parameters, namely structure height h, skewness sk, and kurtosis ks, and one hybrid parameter, i.e. real-to-projected area ratio, or effective area A_{eff}, were used as attributes. These parameters combined provide a general impression of the characteristics of the topography in terms of roughness, shape, symmetry, and increase of effective area [10].

Fig. 1d shows as an example the structure height calculated for each unit cell. After the determination of the four attributes in each unit cell, the Gini coefficient G_i for each attribute i is calculated from the Lorenz curves [29] and the homogeneity relative to each attribute is determined as $H_i = 1 - G_i$. In Fig. 1e, the Lorenz curve corresponding to the structure height distribution of Fig. 1d is shown. In this case, the Gini coefficient was relatively low ($G_{height} = 0.065$) which implies a high homogeneity factor $H_{height} = 0.935$. Finally, the global homogeneity is calculated as the average of the individual homogeneity factors.

3.2 Impact of laser parameters on the texture quality

To illustrate the general trends observed in the topography characterization results, Fig. 2 shows confocal microscopy images and corresponding extracted profiles of selected samples for the three coatings. The labels indicate the number of applied pulses N and the used fluence per pulse F. Namely, in Fig. 2a the impact of the number of applied pulses N on the topography of CrN-coated samples can be observed. Typically, less than 10 pulses per spot yielded low-quality textures with poorly-defined ridges. As N increased to the range 10 – 20 the homogeneity improved and the grooves became deeper. It was noticed that as N increased beyond 20 the amount of molten and redeposited material increased and therefore the texture homogeneity tended to degrade.

In the examples of Fig. 2b, a-C:H coatings were irradiated with increasing fluence per pulse F. Generally, the impact of this parameter is much less significant than the number of pulses, and the optimum value is strongly dependent on the chosen value of N. Interestingly, ablation even took place at fluences below the measured fluence threshold of 0.51 J/cm^2 (see Fig. 2b, leftmost). This finding can be ascribed to incubation effects that reduced the effective threshold fluence to values below 0.22 J/cm^2 [30]. Finally, Fig. 2c shows how the cumulated fluence ($F_{\mathrm{cum}} = N \times F$) influences the topography in WC coatings. If F_{cum} is low, the line-like textures are shallow and not very well-defined. As F_{cum} increases, the homogeneity improves and an optimum region can be determined until, eventually, the cumulated fluence is so high that large amounts of molten and redeposited material redistribute randomly over the surface degrading the final topography. The described impacts of the three process parameters as well as the reduction of the effective threshold due to apparent incubation phenomena were observed in the three analyzed coatings.

As described in section 2.3, each attribute was calculated in each unit cell of the topography images. Fig. 3 shows the a) structure height, b) skewness, c) kurtosis (in log-scale) and d) effective area averaged over all the unit cells as a function of fluence and number of pulses applied on the WC-coated substrate. As expected, when the cumulated fluence increases (top-right corner in the sub-plots), so do the structure height and effective area [31]. However, for the highest F_{cum} the structure height and effective area drop. The skewness (Fig. 3b) and kurtosis (Fig. 3b) have a strong dependence on the number of pulses, but they show negligible variations when the fluence changes. For a low number of pulses ($N < 10$) the skewness is positive and $sk > 1$, which means that the bulk of the material lies below the mean height [32]. This implies that the shape of the texture has open valleys and sharp ridges [10]. For $N \approx 10$, the skewness oscillates in the range $-1 < sk < 1$, implying an approximately symmetric distribution of the material below and above the average height. When the number of pulses is higher than 10, the skewness is negative which suggests that the process induced topographies with broader peaks and narrow valleys, as shown exemplarily in the profile of Fig. 2a (rightmost sample).

In the case of the kurtosis parameter, there are also two clear regimes, i.e. below and above 10 pulses per spot (Fig. 3c). According to its definition, when $ks = 3$ the histogram

of the topography values has a gaussian distribution, which interestingly occurs at $N \approx 10$ (note that $\log(3) \cong 0.477$). When $N < 10$ the kurtosis increases steeply yielding $ks >> 3$ and thus the topographies have a so-called lepto-kurtic distribution. This hints at textures with a large amount of high sharp peaks and deep narrow valleys, as can be observed in the profile of Fig. 2c (leftmost sample). As the pulse number increases beyond 10, the kurtosis takes values in the range $1 < ks < 5$, which can be considered as topographies with an approximately normal distribution of the material. The trends for the four analyzed attributes were also observed for the a-C:H and CrN samples (see Supplementary Information).

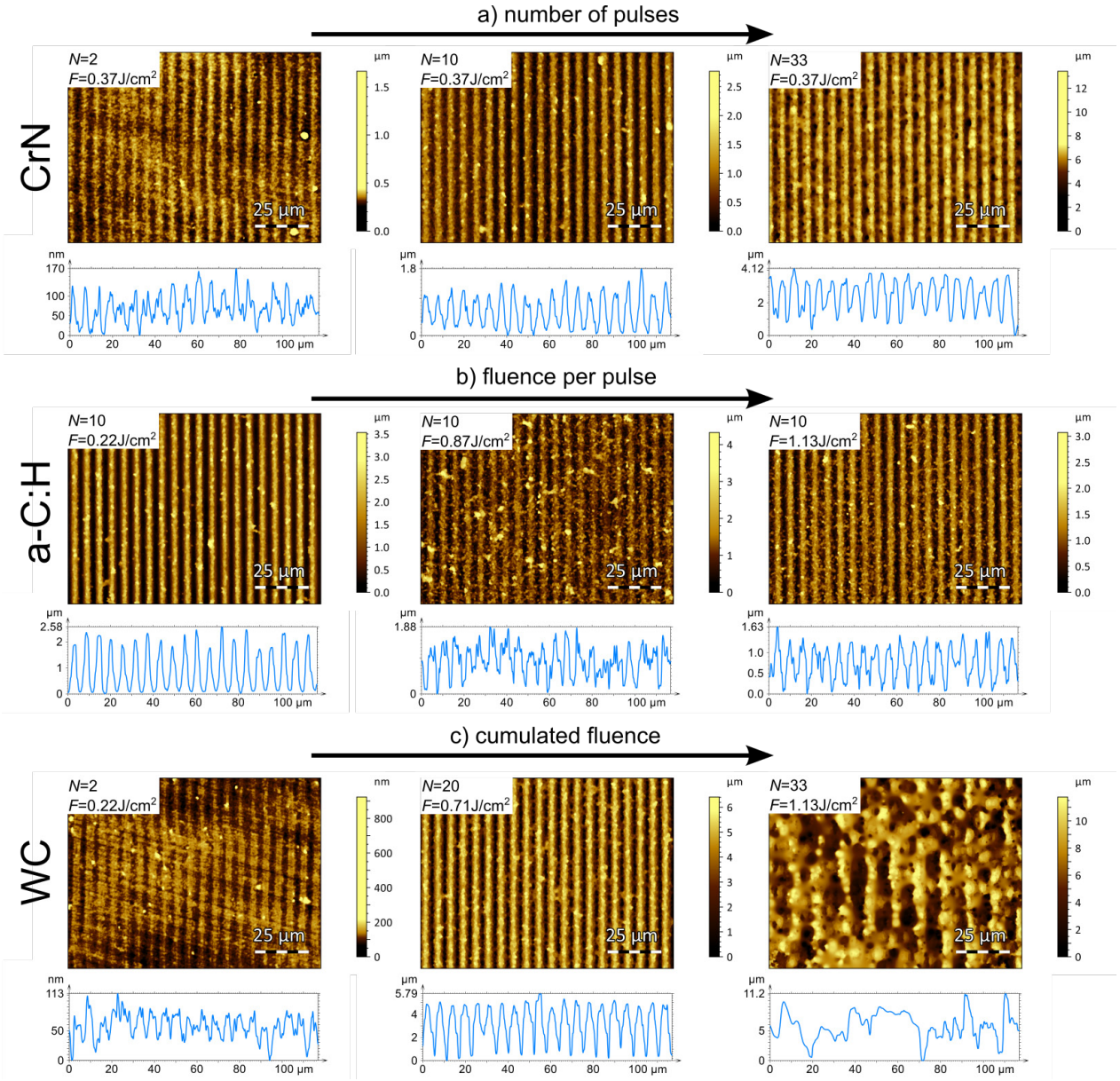

Fig. 2 Topography images and corresponding extracted profiles taken on exemplary samples to illustrate the impact of the number of pulses N and fluence per pulse F on the texture quality.

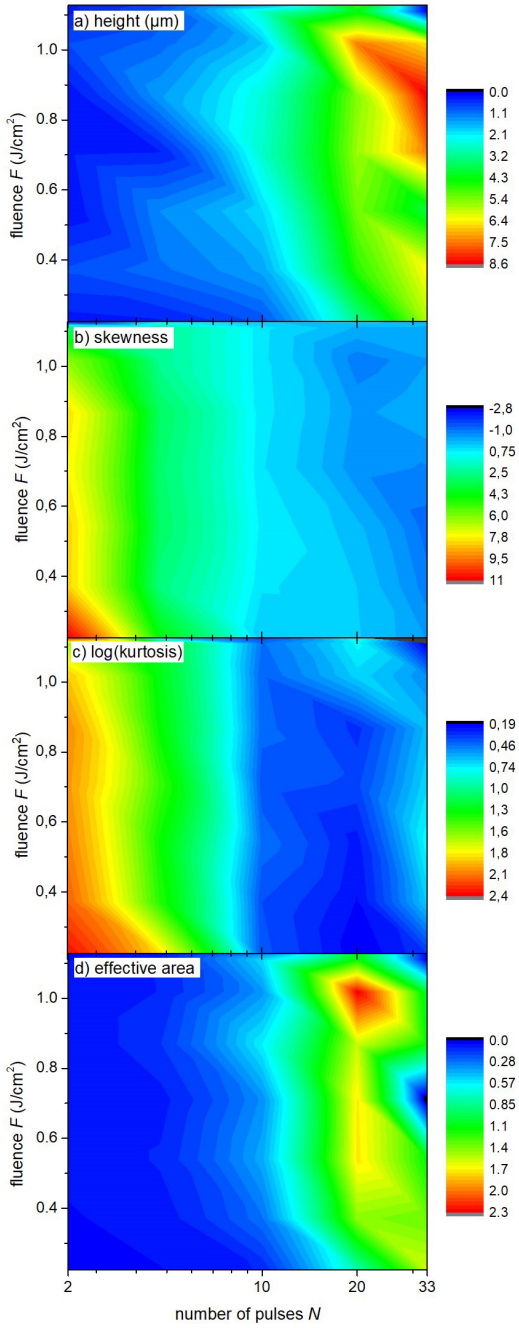

Fig. 3 a) Structure height, b) skewness, c) kurtosis (in log-scale) and d) effective area averaged over all the unit cells as function of fluence per pulse and number of pulses applied on the WC coating system.

3.3 Quantification of homogeneity

Figs. 4, 5, and 6 summarize the main results from the Gini analysis of the WC, a-C:H, and CrN coated substrates, respectively, detailing the homogeneity factors for the a) structure height, b) skewness, c) kurtosis and d) effective area as a function of fluence and number of pulses. The scale of each homogeneity factor is displayed next to each plot. The black color in the plots represents poor-quality textures whose homogeneity could not be quantified with the current method. This limitation was caused by the fact the dominant spatial frequency of the Fourier transform of the topography lies outside the permitted range of allowed frequencies. Hence, this can be interpreted that the topography has such a low quality that the DLIP periodicity is not, or maybe barely, detectable, as it can be seen for example in Fig. 2c (rightmost image). In general, it is observed that the homogeneity factors are strongly influenced by the two analyzed laser parameters as well as by the chosen material. Within the analyzed DLIP parameters range, the three studied coatings systems have an optimum DLIP-processability window that maximizes the surface uniformity. Interestingly, for the three materials the optimum number of pulses for the four homogeneity attributes lies approximately in the range between 10 and 25.

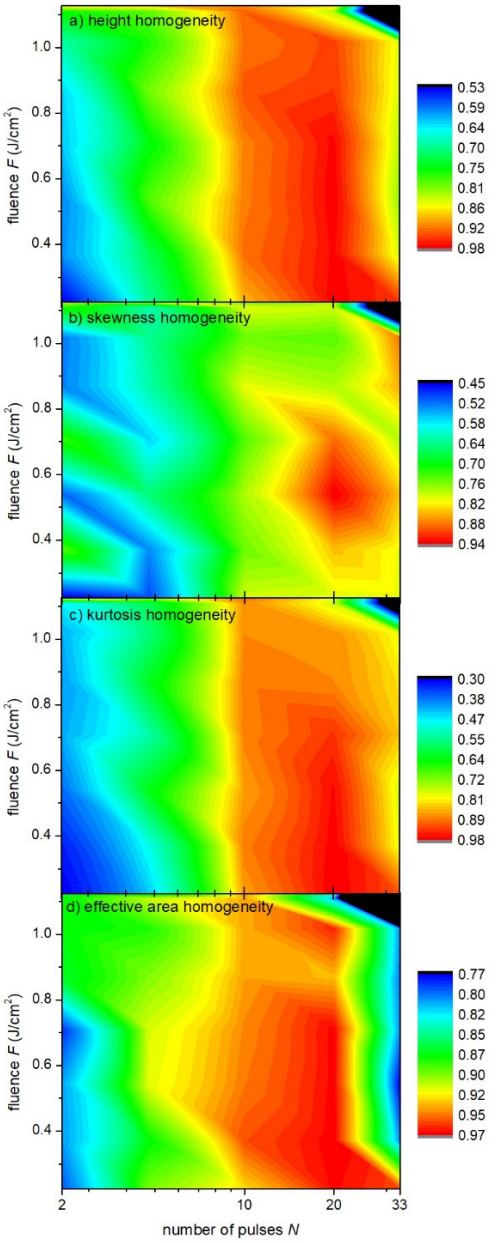

Fig. 4 Homogeneity factors for the a) structure height, b) skewness, c) kurtosis and d) effective area as function of fluence and number of pulses applied on the WC-coated substrate.

Upon comparing the average structure height and effective area (for example Fig. 3a and d) with their corresponding homogeneity factors (Fig. 4a and d) no direct correlation can be established, except for the fact that shallow structures, i.e. lower than 1 µm, tend to have a lower ho-

mogeneity. However, when analyzing the skewness and kurtosis, the results suggest that high values of skewness and kurtosis correlate to low homogeneity factors. From this finding then it can be inferred that the closer the topography histogram to a gaussian one is, then the more homogeneous the periodic textures are.

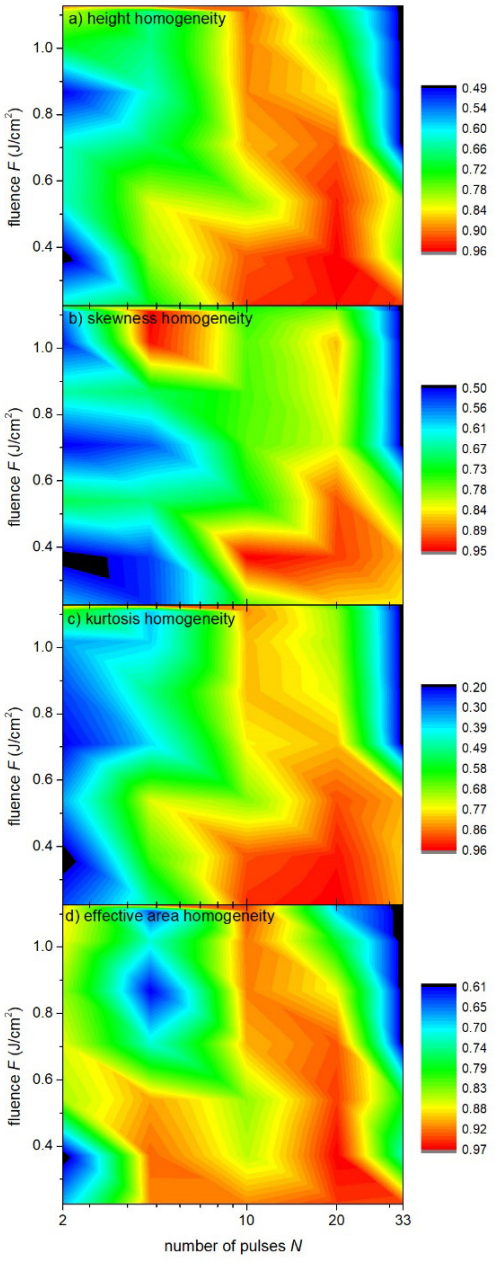

Fig. 5 Homogeneity factors for the a) structure height, b) skewness, c) kurtosis and d) effective area as function of fluence and number of pulses applied on the a-C:H material system.

Particularly, for the CrN samples, the optimum region is narrower than for the WC and a-C:H coatings and more combinations of laser parameters produced less homogeneus textures when compared to the other materials (see the black regions in the top-right corners of the plots in Fig. 6). Further studies on this material should be carried out in order to explain its poorer processability by DLIP.

The global homogeneity was defined in section 2.3 as the arithmetic average of the four homogeneity factors. Fig. 7 shows the global homogeneity obtained for the a) WC, b) a-C:H and c) CrN coatings. Interestingly, the ranges of the global homogeneity for the three materials are very similar (see color scales on the right-hand side of Fig. 7). As was already inferred from analyzing Figs. 4, 5, and 6, the textures have generally higher homogeneities if the number of applied pulses is greater than 10. This claim is also true for the global homogeneity of the three materials. In the case of WC, the optimum processing window is larger than for the other coatings and particularly does not depend strongly on the fluence. In the cases of a-C:H and CrN the optimum fluence values were found to be close to the threshold fluence of these materials, namely approximately in the range 0.3 - 0.5 J/cm^2.

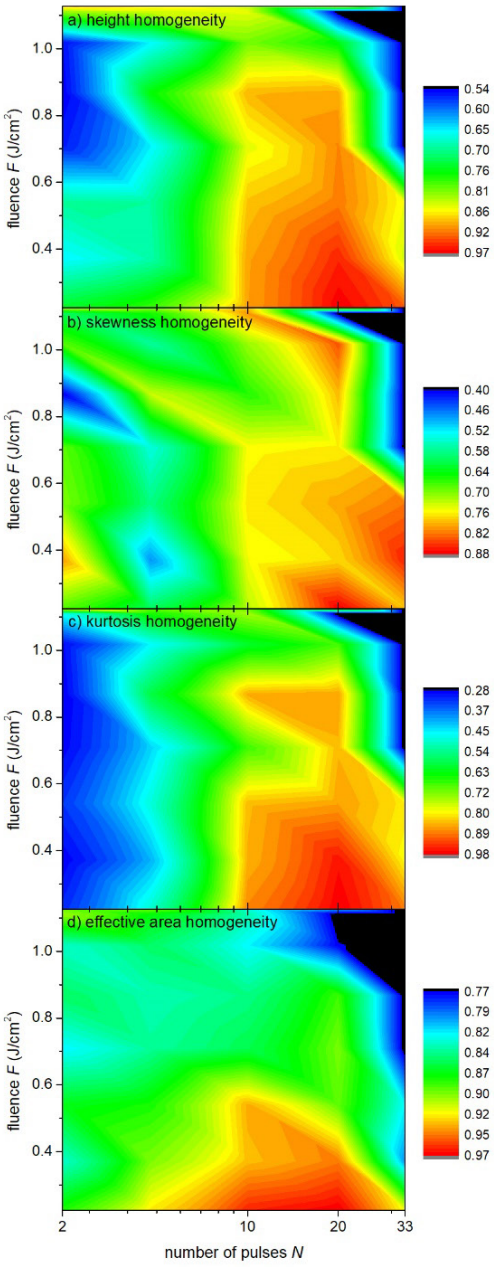

Fig. 6 Homogeneity factors for the a) structure height, b) skewness, c) kurtosis and d) effective area as function of fluence and number of pulses applied on the CrN coating.

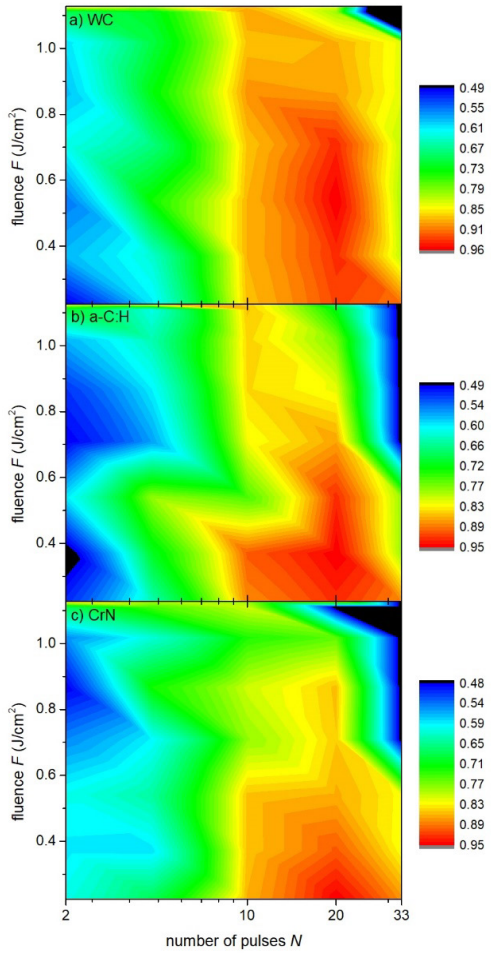

Fig. 7 Global homogeneity calculated on the a) WC, b) a-C:H and c) CrN coatings as function of fluence per spot and number of pulses.

4. Conclusions

In summary, the followed approach based on the Gini statistical analysis allowed for objectively quantifying the homogeneity of periodic textures produced by ps-DLIP. Despite the attributes on which the present study relies were arbitrarily selected, they effectively served as indicators for the texture shape, roughness, and peak-to-valley distance. The method enabled the detection of correlations between the attributes and homogeneity. For instance, analyzing the skewness and kurtosis of the textures, it was found that the closer the distribution of the material heights to a gaussian distribution is, the higher the homogeneity is. Overall, the samples treated with more than 10 pulses per spot showed high homogeneity factors. For the WC coatings, the best processing conditions were obtained for approximately 20 pulses at a fluence in the range from 0.3 J/cm^2 to 0.8 J/cm^2. In the cases of a-C:H and CrN coated substrates, the process window is narrower than in the case of WC because a stronger dependence of the fluence on the texture homogeneity was found. Therefore, for both materials the optimum textures were obtained for approximately 20 pulses at a fluence of 0.3 J/cm^2. It is worth mentioning that the found processing windows with the presented method are subject to other laser parameters that were held constant in this work, such as repetition rate, wavelength or DLIP spatial period. Further studies should be conducted under different DLIP process conditions to find the global optimum process window for each material.

Acknowledgments

This work was supported by the European Union's Horizon 2020 program (M-ERA.NET Joint Call 2020, LUBRICOAT, Reference Number: project8295). The authors would like to thank T. Abraham and M. Weber (Fraunhofer IST) for the preparation of the coating systems.

References

[1] P. Formentín and L. F. Marsal: Nanomaterials, 11, (2021) 670.
[2] M. Laurenti, A. Verna, M. Fontana, S. Stassi, G. Canavese, S. L. Marasso, and V. Cauda: Adv. Mater. Interfaces, 3, (2016) 1600110.
[3] A. Kurella and N. B. Dahotre: J. Biomater. Appl., 20, (2005) 5.
[4] B. Mao, A. Siddaiah, Y. Liao, and P. L. Menezes: J. Manuf. Processes, 53, (2020) 153.
[5] F. Mücklich, A. Lasagni, and C. Daniel: Int. J. Mater. Res., 97, (2006) 1337.
[6] F. Ränke, R. Baumann, B. Voisiat, and A. Fabián Lasagni: Mater. Lett. X, 14, (2022) 100144.
[7] S. Indrišiūnas, B. Voisiat, M. Gedvilas, and G. Račiukaitis: J. Laser. Appl., 29, (2017) 011501.
[8] F. Fraggelakis, G. D. Tsibidis, and E. Stratakis: Phys. Rev. B, 103, (2021) 054105.
[9] L. Mulko, M. Soldera, and A. F. Lasagni: Nanophotonics, 11, (2022) 203.
[10] E. S. Gadelmawla, M. M. Koura, T. M. A. Maksoud, I. M. Elewa, and H. H. Soliman: J. Mater. Proc. Technol., 123, (2002) 133.
[11] B. Lechthaler, C. Pauly, and F. Mücklich: Sci. Rep., 10, (2020) 14516.
[12] A. I. Aguilar-Morales, S. Alamri, T. Kunze, and A. F. Lasagni: Opt. Laser Technol., 107, (2018) 216.
[13] C. He, K. Vannahme, and A. Gillner: J. Laser Micro. Nanoen., 14, (2019) 95.
[14] M. El-Khoury, B. Voisiat, T. Kunze, and A. F. Lasagni: Materials, 13, (2020) 4101.
[15]G. Guillemot, M. Bigerelle, and Z. Khawaja: Scanning, 36, (2014) 127.
[16] S. Teutoburg-Weiss, B. Voisiat, M. Soldera, and A. F. Lasagni: Materials, 13, (2020) 53.
[17] J. Bonse, M. Munz, and H. Sturm: J. Appl. Phys., 97, (2005) 013538.
[18] I. Gnilitskyi, T. J.-Y. Derrien, Y. Levy, N. M. Bulgakova, T. Mocek, and L. Orazi: Sci. Rep., 7, (2017) 1.
[19] S. He, J. J. Nivas, K. K. Anoop, A. Vecchione, M. Hu, R. Bruzzese, and S. Amoruso: Appl. Surf. Sci., 353, (2015) 1214.
[20]A. Forbes, P. Tomlins, E. Gurdak, M. Illsely, S. James, and E. James: J Mater Sci: Mater Med, 21, (2010) 2463.
[21] J. J. Filliben, K. Kafadar, and D. R. Shier: Math. Model., 4, (1983) 167.
[22] O. Oreshkin, A. Platonov, D. Panov, and V. Petrovskiy: Micromachines, 13, (2022) 618.

[23] P. Rossi, M. Engstler, and F. Mücklich: Prakt. Matallogr.-Pr. M, 51, (2014) 180.
[24] P. J. Lambert and J. R. Aronson: Econ. J., 103, (1993) 1221.
[25] O. Stark, J. E. Taylor, and S. Yitzhaki: J. Dev. Econ., 28, (1988) 309.
[26] F. Kuisat, T. Abraham, T. Schmidt, M. Weber, M. Demmler, G. Bräuer, and A. F. Lasagni: J. Laser Micro. Nanoen., 15, (2020).
[27] T. Abraham, I. Bialuch, G. Bräuer, F. Flegler, and P. Groche: JOM, 72, (2020) 2504.
[28] R. Bethke and K. Bewilogua: Materialwiss. Werkst., 35, (2004) 910.
[29] J. Fellman: J. Stat. Econ. Methods, 1, (2012) 31.
[30] J. Byskov-Nielsen, J.-M. Savolainen, M. S. Christensen, and P. Balling: Appl. Phys. A, 101, (2010) 97.
[31] Y. Fu, M. Soldera, W. Wang, B. Voisiat, and A. F. Lasagni: Materials, 12, (2019) 3409.
[32] M. G. Bulmer: *Principles of Statistics*, Courier Corporation, (1979).

(Received: May 17, 2022, Accepted: August 27, 2022)